Applying SMOS Soil Moisture data into the National Weather Service (NWS)'s Research Distributed Hydrologic Model (HL-RDHM) for flash flood guidance application

Dugwon Seo[1] (NOAA-Cooperative Remote Sensing Science and Technology Center)
Tarendra Lakhankar[2] (NOAA-Cooperative Remote Sensing Science and Technology Center)
Brian Cosgrove[3] (NOAA-National Weather Service, Office of Hydrologic Development)
Reza Khanbilvardi[2] (NOAA-Cooperative Remote Sensing Science and Technology Center)
Xiwu Zhan[4] (NOAA Center for Satellite Applications and Research)

[1]Present address of corresponding author, Dugwon Seo (dseo@qcc.cuny.edu)
Queensborough Community College, City University of New York, 222-05 56th Avenue, Bayside, NY 11364

Abstract

After rainfall, soil moisture is the most important factor dictating flash flooding, since rainfall infiltration and runoff are based on the saturation of the soil. However, continuous and regional soil moisture data acquisition is difficult by ground-based measurement. As such, soil moisture is often derived from land surface models and used by agencies such as the National Oceanic and Atmospheric Administration's National Weather Service (NOAA/NWS) as a proxy for estimates of soil moisture at the surface in order to support operational flood forecasting. The current Flash Flood Guidance (FFG) system at the Arkansas Red Basin River Forecast Center (ABRFC) provides gridded flash flood guidance (GFFG) by using the soil moisture from the NWS Hydrology Laboratory-Research Distributed Hydrologic Model (HL-RDHM) to scale Natural Resources Conservation Service curve numbers. This study evaluates the contribution of remote sensing technology to quantifiable improvements in HL-RDHM soil moisture as well as adding a satellite-based soil moisture component to the NWS FFG Algorithm. The Soil Moisture and Ocean Salinity (SMOS) satellite of European Space Agency operates at an L-band (1.4 GHz) wavelength which offers relatively deeper penetration and has lower sensitivity to vegetation impacts than other microwave satellite platforms. It has been shown to be well-suited for observing surface soil moisture. The purpose of this paper is to determine, execute, and assess a method of SMOS data assimilation applicable for use with the HL-RDHM modeling system. The value of remote sensing data in constraining modeled soil moisture states is evaluated. Results from the technique developed in this study imply a potential for SMOS-based improvement of the GFFG product. The technique is also expected to be useful for assimilating soil moisture data from the Soil Moisture Active Passive (SMAP).

Keywords

SMOS; L-band; Soil moisture; Gridded Flash Flood Guidance; HL-RDHM; Hydrologic modeling

1. Introduction

Soil moisture interacts with the atmosphere through evaporation and transpiration, and drives infiltration and runoff during heavy rain events. The available water storage capacity in the soil column influences the amount of runoff and the potential for flash floods. Flash flooding is a rapid water level rise in a stream above a predetermined flood level, beginning within six hours by intense rainfall associated with severe weather phenomena, or the collapse of a dam. In the U.S., losses over 30 years have averaged 8.2 billion dollars in damage and 89 fatalities per year according to the flood loss data in the Hydrologic Information Center (HIC) database (http://www.nws.noaa.gov/oh/hic/). The number of fatalities and damage to property likely could have been reduced if additional advance notice of potential flash flooding had been provided. In spite of the deadly impact of flash floods, they are relatively poorly observed and forecasted (Seo et al., 2013) compared to other natural hazards (Gruntfest, 2009).

Given the close ties between the state of the soil column and flash flooding, reliable soil moisture information would help to improve flash flood forecasts. Unfortunately, the current main sources of soil moisture data--ground-based measurements and hydrologic models--provide only limited insight into the overall state of soil moisture. Conducting ground-based measurements of soil moisture consistently and regionally is difficult, and obtaining comparable soil moisture from hydrologic models is complicated in both structure and parameterization (Houser et al., 1998). Remote sensing-based platforms provide a strong alternative and are less subject to spatial coverage limitations (Jackson et al., 1999), and with microwave remote sensing, soil moisture can be estimated from the emissive and scattering characteristics of the soil surface.

The application of remote sensing to measure soil moisture has been researched over the last thirty years using both passive and active microwave instruments (Ulaby et al.,1981). Microwave remote sensing at low frequencies is well-suited for estimating soil moisture since it is very sensitive to the dielectric properties of the soil (Jackson et al., 1995). The low frequency microwave spectrum has the advantage of deeper penetration and is less subject to atmospheric effects. Two microwave satellite missions, the ESA Earth Explorer SMOS (Soil Moisture and Ocean Salinity) launched on November 2009 and NASA's SMAP (Soil Moisture Active Passive) scheduled to launch in December 2014, take advantage of low microwave frequencies for remote sensing of soil moisture. The previous SMOS assimilation research showed that the peak runoff observations were improved when SMOS soil moisture was applied providing soil moisture conditions which implies the potential benefit of SMOS soil moisture data in the forecasting of floods (Lievens et al., 2015).

In this study, a method of assimilating SMOS soil moisture into the National Weather Service's HL-RDHM is established to support improved soil moisture simulations and associated flash flood applications in the Arkansas-Red River basin. SMOS soil moisture data at a 0.25 degree resolution processed at NOAA NESDIS was obtained and downscaled to the 4 km x 4 km HL-RDHM grid typically used by the NWS for distributed hydrologic modeling. For the purpose of flash flood forecasting, moisture content information from the surface down through the root zone of the soil column (around 50 cm to 100 cm from the surface) is crucial. Also, since flash floods occur on short time scales, hourly soil moisture information is important for flash flood analysis and forecasting applications. However, SMOS only provides soil moisture content to a depth of a few centimeters (Bircher et al., 2012) and features a 2 to 3 day revisit time. Insertion of the snapshot-type surface data from SMOS into HL-RDHM provides the vehicle needed for blending the accuracy of observations with the expanded depth and increased temporal frequency that a model can offer.

Remotely sensed satellite soil moisture is expected to improve current hydrologic analysis and forecast systems, including flash flood forecasts which depend on rapidly updated information. The ultimate goal of this study is to create the framework for satellite based soil moisture assimilation into HL-RDHM, which will in turn benefit the GFFG system which depends on HL-RDHM output.

2. Downscaling of SMOS data

2.1 Dataset

The dynamics and distribution of surface soil moisture are controlled by variables such as soil properties, vegetation characteristics, topography, land surface temperature, solar radiation, and precipitation and have commonly been used in many downscaling techniques. This study was focusing on the development of the technique to utilize SMOS satellite data into hydrologic model for flash flood guidance. Downscaling work was unavoidable to prepare the SMOS data to be suitable to the HL-RDHM which functions for Arkansas-Red River basin gridded flash flood guidance. The downscaling method in this study meant to be as simple as possible using three variables only so the objective of the study remains to focus on promoting satellite soil moisture data on the flash flood application. Advanced downscaling methods can be adopted in the future study from other studies including that for use in hydrologic studies (Kaheil et al., 2008), that using meteorological data (Merlin et al., 2005; Merlin et al., 2006; Piles et al., 2011), that utilizing high-resolution land surface properties (Pellenq et al., 2003; Shin & Mohanty, 2013), that using thermal Moderate Resolution Imaging Spectroradiometer (MODIS) data (Lievens et al., 2016) and that reproduce the statistical properties of soil moisture (Mascaro et al., 2010; Ko et al., 2016).

In this study, keeping it simple but considering the availability of directly measured data through remote sensing, three dominant physical controls--sand fraction, vegetation characteristics by Normalized Difference Vegetation Index (NDVI) and elevation--were selected to estimate SMOS soil moisture at the high resolution 4km study scale. These three geophysical attributes are proxies for other significant attributes such as slope, aspect, vegetation water content, and soil type (Das et al., 2014).

Soil moisture content and movement are affected by soil texture since the hydraulic conductivity and water holding capacity of the soil depend on sand fraction. Soils with a higher sand fraction will have a higher infiltration rate and evaporative flow. This typically leads to a lower soil moisture content and illustrates the inverse covariance of soil moisture with sand fraction. Sand fraction was acquired from the International Soil Reference and Information Center (ISRIC) world soil information database. The dataset provides global information at a 5 arc minute (~ 9km) resolution but was rescaled to 4 km. Sand fraction data from the study area (Arkansas Red River basin) at a 0-20 cm depth was extracted for this study.

Thirty arc second elevation data was acquired from the GTOPO30 global digital elevation model (DEM), developed by the U.S. Geological Survey (USGS). Typically, higher elevation areas are drier than lower elevations due mainly to the effect of gravity (Henninger et al., 1976). This topographic effect is most visible in the upper layer of the soil. As with sand fraction, elevation and soil moisture are thus inversely related. The elevation of study area is relatively high in the west and gradually decreases toward the east.

NDVI is a strong indicator of vegetation status over time and has a positive correlation to soil moisture. The higher vegetation density increases biomass, fallen leaves, and soil organic matter that preserve the moisture in soil. Also, the vegetation cover helps to decrease evaporation by screening the sun (Das et al., 2014). In order to capture the seasonal dynamic characteristics of vegetation effects, monthly NDVI were included in the downscaling technique. For the variable vegetation status, monthly NDVI dataset was obtained from MODIS. The NDVI dataset also shows the east side of study area is seasonally more variable than the west.

The SMOS soil moisture product was obtained from NOAA's National Environmental Satellite Data and Information Service (NESDIS), after they reproduced data in 0.25 degree using their algorithm. This 0.25 degree (~25km) dataset was used as the core soil moisture in this study.

2.2 Methodology

SMOS soil moisture is downscaled using Equations 1(a), (b), (c) and Equation 2 (Das, 2014) with the physical control parameters described in previous section (2.1). $SF(i)$, $EL(i)$, and $NDVI(i,t)$ are the sand fraction, elevation and monthly normalized difference vegetation index respectively at the original scale at which the data was obtained, and $SF_{w\_4km}(i)$, $EL_{w\_4km}(i)$, and $NDVI_{w\_4km}(i,t)$ are weighted values at a 4km resolution. $SM_{4km}(i,t)$ is the downscaled 4km SMOS soil moisture at location i and at time t. SM_{25km} is SMOS soil moisture at 25 km resolution, and m is the number of 4 km pixels within a 25 km grid cell. Equation 2 represents the combined effect of the physical controls on the evolution of surface soil moisture, including the negative covariance of the sand fraction and elevation, and the positive covariance of NDVI. The physical control parameter terms ($1/SF_{w\_4km}(i)$, $1/EL_{w\_4km}(i)$, and $NDVI_{w\_4km}(i)$) were simply averaged and then multiplied by the coarse resolution SMOS soil moisture value (Das, 2014).

$$SF_{w\_4km}(i) = SF(i) / \frac{1}{m}\sum_{i=1}^{m} SF_{4km}(i) \qquad \text{Equation 1(a)}$$

$$EL_{w\_4km}(i) = EL(i) / \frac{1}{m}\sum_{i=1}^{m} EL_{4km}(i) \qquad \text{Equation 1(b)}$$

$$NDVI_{w\_4km}(i) = NDVI(i) / \frac{1}{m}\sum_{i=1}^{m} NDVI_{4km}(i) \qquad \text{Equation 1(c)}$$

$$SM_{4km}(i,t) = SM_{25km} \times \frac{1}{3}\left[\frac{1}{SF_{w\_4km}(i)} + \frac{1}{EL_{w\_4km}(i)} + NDVI_{w\_4km}(i,t)\right] \qquad \text{Equation 2}$$

Figure 1 shows the image of the original coarse resolution (25km) and post-downscaling fine resolution (4km) SMOS soil moisture. Considerable sub-pixel variability is obtained via this downscaling process. For example, while one sample coarse SMOS pixel has a volumetric value of 0.59, the corresponding 6 x 6 set of downscaled pixels have a standard deviation of 0.06.

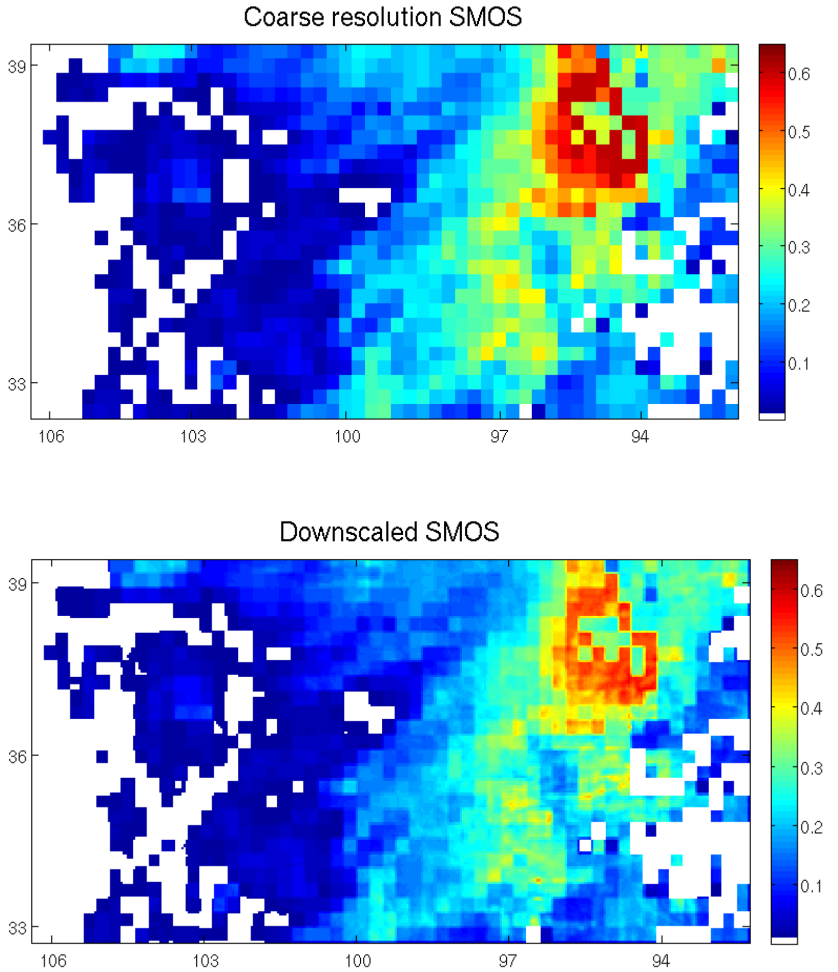

Figure 1 SMOS soil moisture pixels image comparison at coarse (25km) resolution (top) and downscaled (4km) resolution (bottom). The image map shows soil moisture in study area of Arkansas-Red river basin on May 13th, 2010

2.3 Bias Correction

2.3.1 Comparison of SMOS retrievals to in situ Soil Moisture Measurements

In support of assessing the suitability of SMOS soil moisture for use in the assimilation process, a brief validation study was carried out comparing the coarse and downscaled SMOS soil moisture against in situ measurements. Soil moisture measurements were obtained from the U.S.

Climate Reference Network (USCRN) data distributed by the NOAA National Climate Data Center. Many USCRN stations are equipped to observe relative humidity, soil moisture and soil temperature (Diamond et al., 2013). The Goodwell and Stillwater sites in Oklahoma and Joplin in Missouri were selected as study stations within the Arkansas-Red river basin. Since the La Junta station in Colorado does not have available soil moisture data, it was not included as a validation site. Daily and hourly time-averaged 0-5cm fractional volumetric soil moisture was obtained for 2010. This observation depth was chosen as it most closely matches the depth observed by SMOS using its L-Band microwave radiometer (Kerr et al., 2010, Kerr et al., 2012, Entekhabi et al., 2010). Geologic, climate, and physical soil characteristics for the three stations are listed in Table 1 (Bell et al., 2013, www.weatherbase.com). It should be noted that the Goodwell site features different characteristics compared to other two sites; lower average soil moisture and precipitation along with lower soil bulk density which is related to high porosity. Moreover, it was verified via satellite images that the vegetation coverage at the Goodwell site is less dense than that at Stillwater and Joplin.

Daily point-type soil moisture measurements from USCRN, 25km gridded SMOS soil moisture, and downscaled 4km gridded SMOS soil moisture were validated in a time series fashion from May 4th to December 31st, 2010. SMOS data at both scales display drying and wetting similar to the USCRN measurements, yet the values are mostly negatively biased as shown in Figure 2 (-0.065, -0.100, and -0.112 at Goodwell, Stillwater and Joplin respectively). Several validation studies were reviewed (Al Bitar et al., 2012; Jackson et al., 2012; Lee et al., 2002;), with each indicating that a comparison of SMOS soil moisture and in situ measurements from different sources yielded negative biases. These studies commonly stated that the variation of errors depended on vegetation coverage and the wetness of the climate (Pan et al., 2012; Albergel et al.

2012). The validation of SMOS soil moisture conducted for this study indicated the best overall USCRN-SMOS match occurred at Goodwell (dry climate and low vegetation cover). Given the preceding findings, it was necessary to bias correct the SMOS data before assimilation into HL-RDHM. The data adjustment methodology underpinning the bias correction is explained in the following section.

Table 1 Geologic, climate and soil information at three stations

Stations	**Goodwell, OK**	**Stillwater, OK**	**Joplin, MO**
Latitude	36.59	36.12	37.43
Longitude	-101.59	-97.09	-94.58
Average measured soil moisture from USCRN (cm^3/cm^3)	0.13	0.24	0.30
Annual average precipitation (mm)	406.4	850.9	967.7
Surface description	Low prairie grass	Grass	Grass
Soil description	Sandy	Hard sand	Sand/Organic matter
Soil Bulk Density (g/cm^3)	0.13	0.24	0.30
Bias	-0.065	-0.100	-0.112
Average NDVI	0.39	0.66	0.69

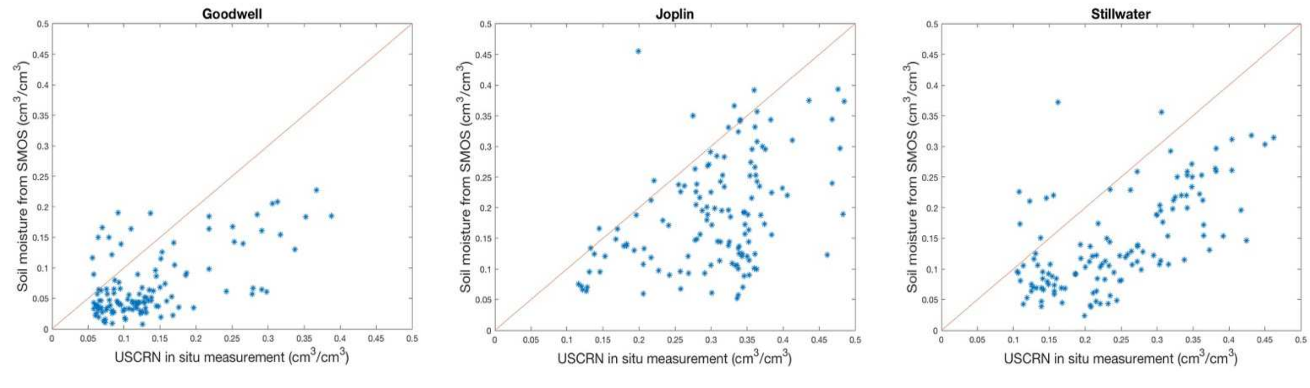

Figure 2 Negative biased SMOS soil moisture compared to USCRN in situ measurement

2.3.2 Bias Correction

The aim of the SMOS mission is to provide high accuracy and resolution surface soil moisture observations using innovative microwave L-band technology (Kerr et al., 2001). However, the negative biases inherent in the SMOS soil moisture observations complicate their use in hydrologic data assimilation. With bias correction unavoidable, a statistical correction using mean and variance was applied to adjust the data before use in HL-RDHM.

Under the statistical correction technique, the distribution of a reference source (e.g. modeled distribution) is matched to, and corrects, the distribution of the desired data set (Choi and Jacobs, 2008). USCRN and HL-RDHM datasets (smc1-soil moisture content at the first layer from surface) were both considered as reference sources. Patterns in the top layer soil moisture estimates from HL-RDHM matched those present in the USCRN data, yet the data range was overly low. It overestimated soil moisture during dry periods and underestimated during wet periods as shown in Figure 3. USCRN measurements also present a promising pool of data, but are limited by the small number of measurement sites. To counter the datasets' weak points, HL-RDHM 4km soil moisture was averaged with a kriging-based interpolated USCRN data (Figure 4) to produce a reference source. The kriging method weights the surrounding measured values from USCRN to derive a prediction for an unmeasured locations shown in Equation 3, where $Z(s_i)$ is the measured value at the i^{th} location, λ_i is an unknown weight for the measured value at the i^{th} location, S_0 is the prediction location and N is the number of measured values.

$$Z(S_0) = \sum_{i=1}^{N} \lambda_i Z(S_i) \qquad \text{Equation 3}$$

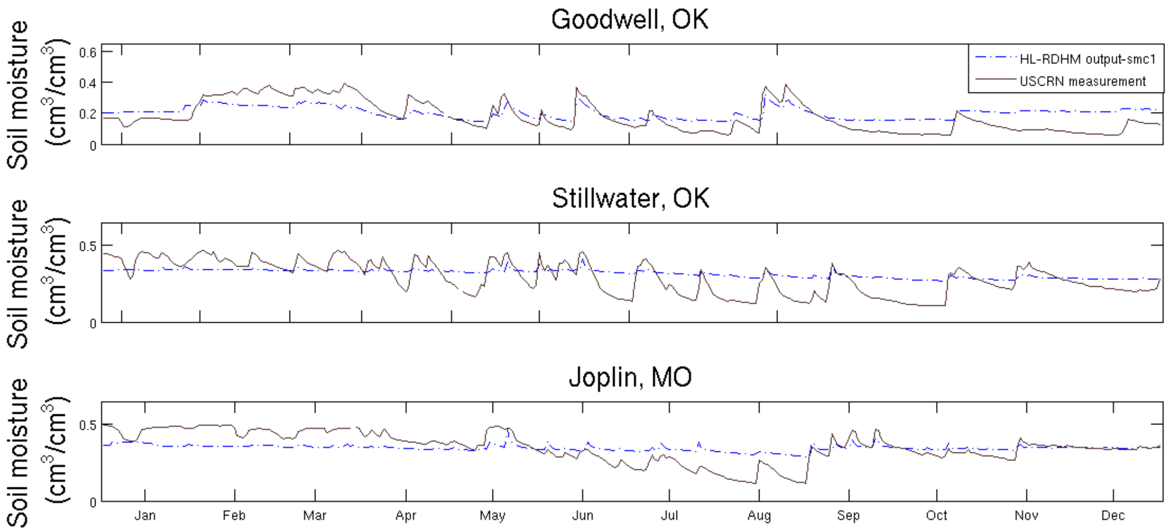

Figure 3 Comparison of daily soil moisture between HL-RDHM output *smc1* (5 to 10 cm depth) and USCRN in situ measurements from the surface to 5 cm for 2010.

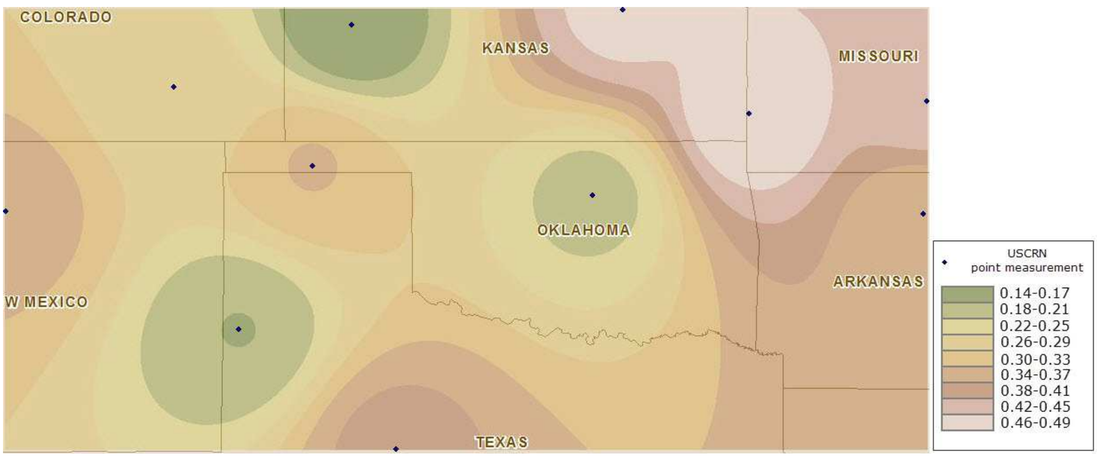

Figure 4 Interpolated USCRN soil moisture measurements (cm^3/cm^3) from 10 sites over the Arkansas-red river basin on May 13th, 2010

Corrected SMOS soil moisture values are derived using Equation 4 where X_t is the corrected SMOS soil moisture value, x_t is the downscaled SMOS soil moisture at time *t*, $\overline{x_t}$ and $\overline{y_t}$ are the means of the downscaled SMOS and merged reference soil moisture respectively, and

$\sigma(x_t)$ and $\sigma(y_t)$ are the standard deviations of the downscaled SMOS and merged reference soil moisture respectively.

$$\boldsymbol{X_t} = \bar{\boldsymbol{y}}_{\boldsymbol{t}} + \frac{\boldsymbol{\sigma(y_t)[x_t - \overline{x_t}\,]}}{\boldsymbol{\sigma(x_t)}} \qquad \text{Equation 4}$$

Figure 5 adds a trace for bias corrected SMOS data which verifies best during wet periods. This behavior stems from the fact that the non-corrected SMOS soil moisture observations matched the USCRN in situ relatively well during dry periods (e.g. the beginning of October in Goodwell and Stillwater sites and between July 15^{th} and August 15^{th} at the Joplin site). Thus the statistical correction technique shifted up the negatively biased data to USCRN measurement values mostly during wet periods but resulted to overestimate soil moisture during these periods.

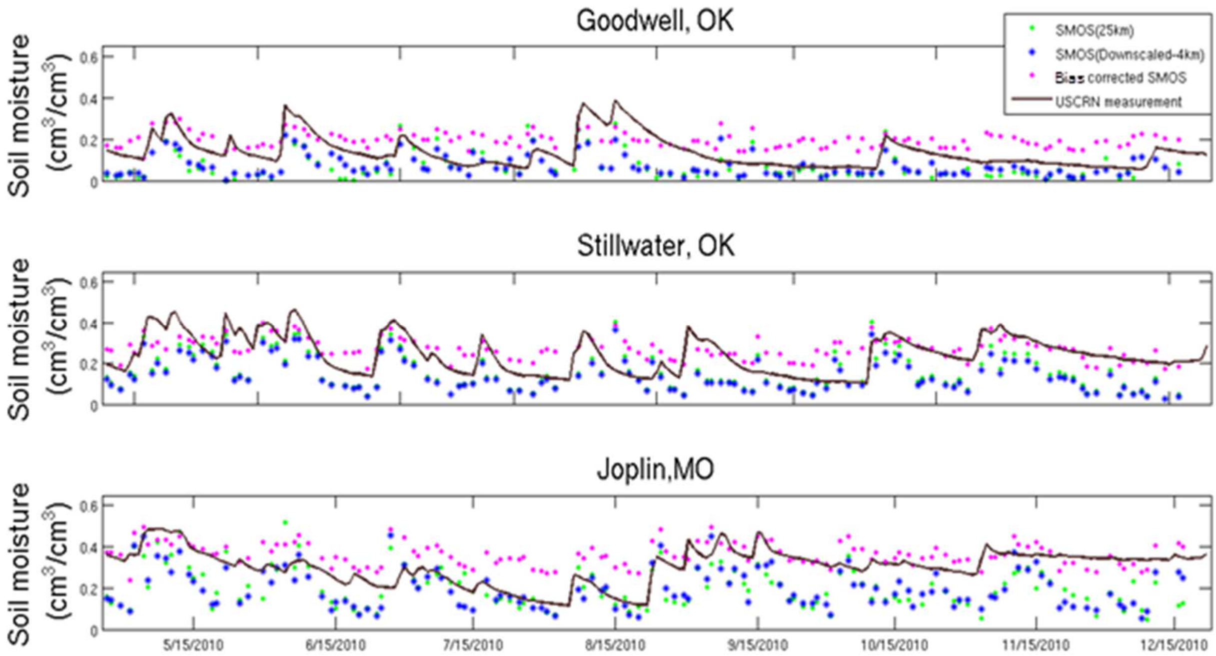

Figure 5 Comparison of SMOS soil moisture data at coarse resolution (25 km) and fine (4km) resolutions, bias corrected, and USCRN measurements for the three sites.

3 Integration of SMOS retrievals to HL-RDHM

Raw SMOS soil moisture data has spatial, vertical and temporal characteristics that make it ill-suited for use with the NWS's operational hydrologic forecast system without data pre-processing. Having previously covered the spatial downscaling of this data in Section 2, this section further describes the necessary pre-processing steps along with the assimilation procedure used to ingest SMOS data into the HL-RDHM system.

While the L-band wavelength is well-suited for soil moisture sensing compared to other microwave wavelengths (Mascaro & Vivoni, 2012), the sensing depth at this frequency is still limited to approximately 5 cm (Escorihuela et al., 2010). Unfortunately, land-atmosphere interaction processes are highly dependent on the profile of soil moisture in the deeper root zone (Houser et al., 1998). Numerous promising approaches for estimating the soil moisture profile have been demonstrated (Bruckler and Witono, 1989; Entekhabi et al., 1994; Crow et al., 2008). With a requirement to maintain compatibility with existing NWS hydrologic modeling systems and the GFFG product, it was decided to use a direct insertion technique in conjunction with existing soil profile rebalancing tools offered by HL-RDHM's Sacramento Soil Moisture Accounting model, versions of which underpin GFFG and other hydrologic operations within the NWS.

HL-RDHM is currently executed on rectangular Hydrologic Rainfall Analysis Project (HRAP) grid. This grid is based on a polar stereo graphic map projection with standard latitude of 60° North and longitude of 105° west. The grid size is approximated as 4 km (http://www.nws.noaa.gov/ohd/hrl/nwsrfs/users_manual/part2/_pdf/21hrapgrid.pdf). Each grid cell consists of a water balance component and hillslope and channel routing component. The water balance component of the HL-RDHM uses the SAC-SMA and kinematic wave model is employed for hillslope channel routing (Koren et al., 2004).

SAC-SMA is a semi-conceptual model of soil moisture accounting that uses empirical and lumped coefficients to attempt to mimic the physical constraints of water movement in a natural system (Burnash, 1995). SAC-SMA basically operates on two layers, upper zone and lower zone. Each zone consists of tension and free water storages that represent the soil column's water holding capacity. The free water storage in lower zone is divided into two sub-storages which control supplemental and primary ground water flows. Figure 6 illustrates a structure of water storages that interact with tension and free water to generate soil moisture states and runoff components in SAC-SMA. Tension water is held in place by the molecular attraction between soil particles and water and can be separated from the soil and returned to the atmosphere through evapotranspiration. Upper zone is active and permeable layer near surface which is mainly the source of the most storm runoff. Upper zone tension water represents that volume of precipitation which moisturizes soil and precedes the development of interflow and percolation. Free water is liquid state that is not bound to soil particles so percolates through the soil to replenish soil moisture deficiency in response to gravitational and pressure forces (Burnash, 1995). In Figure 6, the precipitation will fill up the upper zone tension water storage (*UZTWM*) as upper zone tension water contents at level 1($uztwc_1$) rise to level 2 ($uztwc_2$). The excesses upper zone tension water infiltrates to the upper zone free water storage (*UZFWM*) and replenish from level 1($uzfwc_1$) to level 2 ($uzfwc_2$). HL-RDHM outputs the water contents (*uztwc, uzfwc*) in fractional unit which varies from 0 to 1 where 1 is saturated. When the upper zone saturation demand is satisfied, surface runoff occurs in fast response and interflow occurs slowly from the upper zone free water storage at daily withdrawal rate (*UZK*). Available water after surface runoff from precipitation percolates down to the lower zone when the upper zone soil moisture deficit is less than the amount of precipitation. The same mechanism will work in lower zone tension (*LZTWM*) and free water storage where supplies moisture to meet the evapotranspiration demands. Free water storage in lower zone is divided into supplemental and primary (*LZFSM, LZFPM*) and creates the slow response water movements including supplemental and primary ground water runoff and channel base flow.

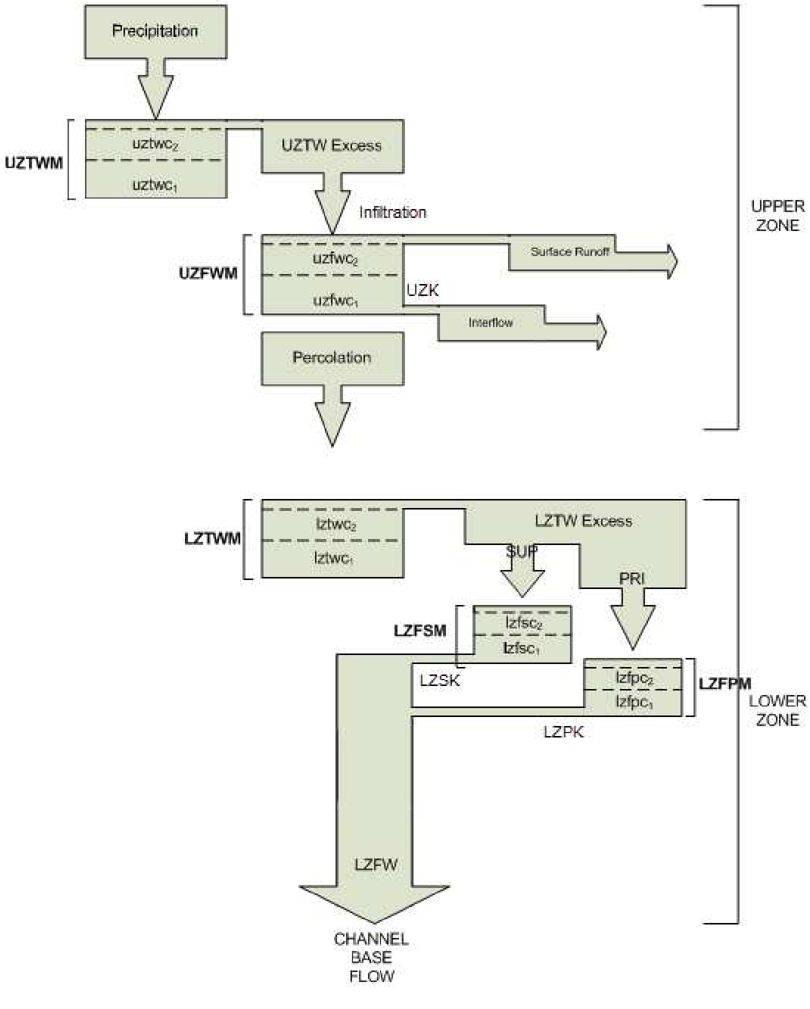

Figure 6 SAC-SMA soil moisture interaction diagram

The most recent version of the Sacramento model available within the HL-RDHM modeling framework, SAC-HTET (Sacramento Heat Transfer with enhanced Evapo Transpiration) (Koren, et al., 2010), was selected for use in this research. SAC-HTET is modified version of SAC-SMA and SAC-HT which includes a physically-based treatment of evapotranspiration adapted from the Noah land surface model (LSM). The physical soil layer definitions of SAC-HTET were leveraged to ensure incorporation of SMOS soil moisture at the proper layer. The soil moisture state is named by the model as *smc0, smc1, smc2, smc3* and *smc4* at each physical soil layer *frz_0, frz_1, frz_2, frz_3* and *frz_4*. Depths and number of layers in SAC-HTET vary spatially as soil texture varies. *frz_0* is a constant value as 3 cm of depth which represent the interception, *frz_1*varies -5 to -16 cm and *frz_2* varies -16 to 63 cm over the study area watershed. The main advantage of using SAC-HTET for this study is the model's revised upper and lower zone soil water redistribution process (Koren et al., 2010) which provides a link between the physical and conceptual soil layers. This is especially important for assimilation, as a path is needed to carry the observed satellite soil moisture from the physical layer model entry point, to the conceptual zones where runoff processes are executed.

In SAC-HTET, evaporative and freeze-thaw processes are calculated using the model's physical soil layers while rainfall runoff processes are calculated using the model's upper and lower zone conceptual storage reservoirs. Using the model's physical layers as an entry point, SMOS soil moisture data was assimilated into the *smc1* layer using the direct insertion technique (Figure 7). In order to ensure consistency between the model's conceptual and physical sides during the soil moisture assimilation process, and to update the profile of the soil column, a SAC-HTET function was utilized to translate soil moisture content in the model's physical layers to the model's upper and lower zone conceptual storage reservoirs. This mapping function works by first dividing the physical layers between upper and lower zones. The total amount of water contained within the two groups of physical layers is then computed and used to scale the original amount of water contained in the upper and lower storage reservoirs. In this way, it was possible to draw SMOS data into the rainfall runoff calculations that form the center of the model. This direct insertion process was repeated each time SMOS data was available to overwrite existing values of *smc1*.

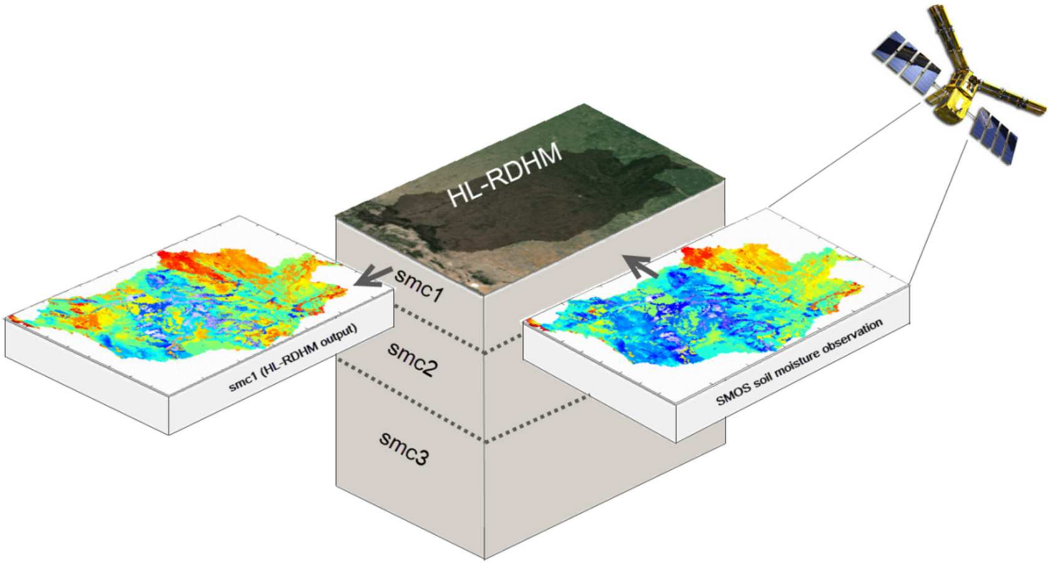

Figure 7 Illustration of SMOS soil moisture assimilation into HL-RDHM/SAC-HET. SMOS soil moisture observation replaces the soil moisture content of the first layer (smc1), which is output from the previous HL-RDHM run.

Before any assimilation experiments were carried out with HL-RDHM, a two year (October 2008 through May 2010) cold start spin-up run was conducted. Drawing all initial conditions except top layer soil moisture (*smc1*) from the end of this spin-up run, the first SMOS assimilation run was started in a warm-start fashion at 00Z on May 4^{th}, 2010. Top layer soil moisture conditions were taken directly from prepared (downscaled and bias corrected) SMOS soil moisture observations, with this data completely replacing the pre-existing model-based *smc1* data field. After the data replacement, HL-RDHM was executed for a 24 hour period, at the end of which model states were saved to serve as initial conditions for the next day's simulation. Beginning the second simulation day, the SMOS-based *smc1* field was once again substituted for the model-based *smc1* field, and a second 24-hour run was executed. This 24 hour run cycle was repeated for the entire study period, with warm-start runs initializing once every 24 hours using data from the previous day's run along with SMOS soil moisture data. A parallel set of 24-hour runs was conducted without SMOS assimilation to provide data for comparison.

While sub-daily remotely sensed soil moisture information would be desirable for enhancing flash flood-related hydrologic modeling systems, the revisit period of SMOS for the same location is only every 2 to 3 days (Kerr et al., 2010). In particular, as Figure 8 displays, SMOS data covers only part of the study basin (ABRFC) each day. Since a spatially complete soil moisture data set is required to initialize HL-RDHM, areas without available SMOS observed soil moisture were filled in using existing *smc1* pixels from the previous model state.

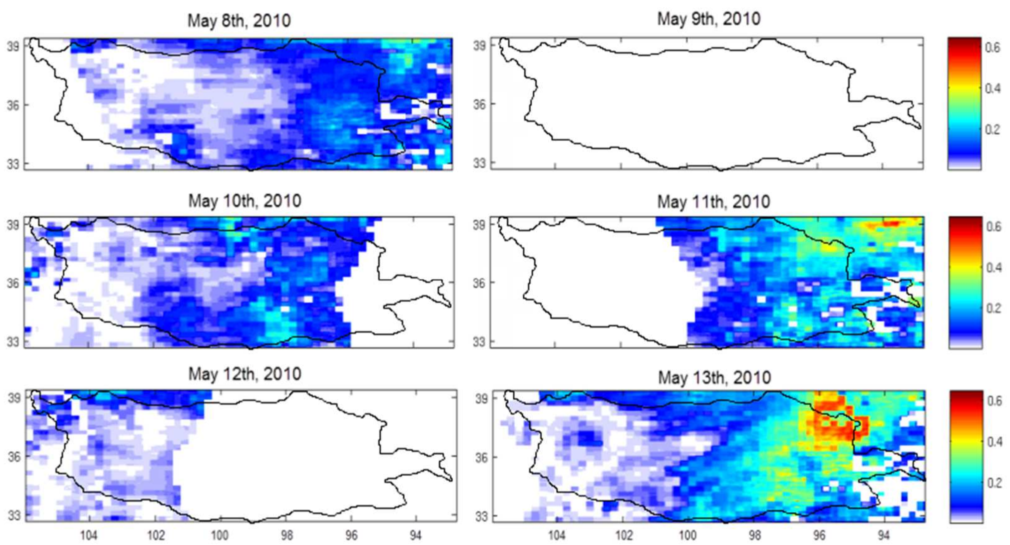

Figure 8 Six consecutive daily SMOS soil moisture images over the study area from May 8th to May 13th 2010

4 Results and Discussion

4.1 Time Series Comparison and Analysis

Several comparison analyses of HL-RDHM soil moisture with and without SMOS assimilation were carried out. In the first analysis, hourly simulated 5-10cm soil moisture (with assimilation) is plotted against USCRN measurements at the same depth from May, 2010 to December, 2010. As depicted in Figure 9, top layer modeled soil moisture resulting from the assimilation of SMOS data closely follows the actual SMOS observations at the Goodwell site. While the match is not as good at the Stillwater site, the with-SMOS simulation matches the dry conditions indicated by the USCRN measurements better than the without-SMOS simulation, which does not fall below a value of 0.32 cm^3/cm^3. It is worth mentioning that even though SMOS-sensed low values of soil moisture were assimilated into the top layer of the model, the model subsequently moistened this layer over a matter of hours until it reached the model's lower soil moisture limit value of 0.32 cm^3/cm^3 (wilting point). For this reason, the red line (with SMOS assimilation) tends to return to the blue line (without SMOS assimilation) after SMOS observations are inserted. Similar behavior can be noted in the Joplin time series plot.

During some periods of precipitation over the Joplin site, SMOS observations indicate relatively wet conditions that run contrary to the USCRN-based measurements. This is indicative of the uncertainty that arises in a comparison between point-type data (USCRN measurement) and area-averaged data (16 km^2 HL-RDHM output). Another source of uncertainty centers on the SMOS soil moisture data we used in the study. Although SMOS descending data (1800 local time) is more error prone (Dente et al., 2012; Jackson et al., 2012) the data used in this study was a NESDIS daily composite and not separated into ascending and descending groups.

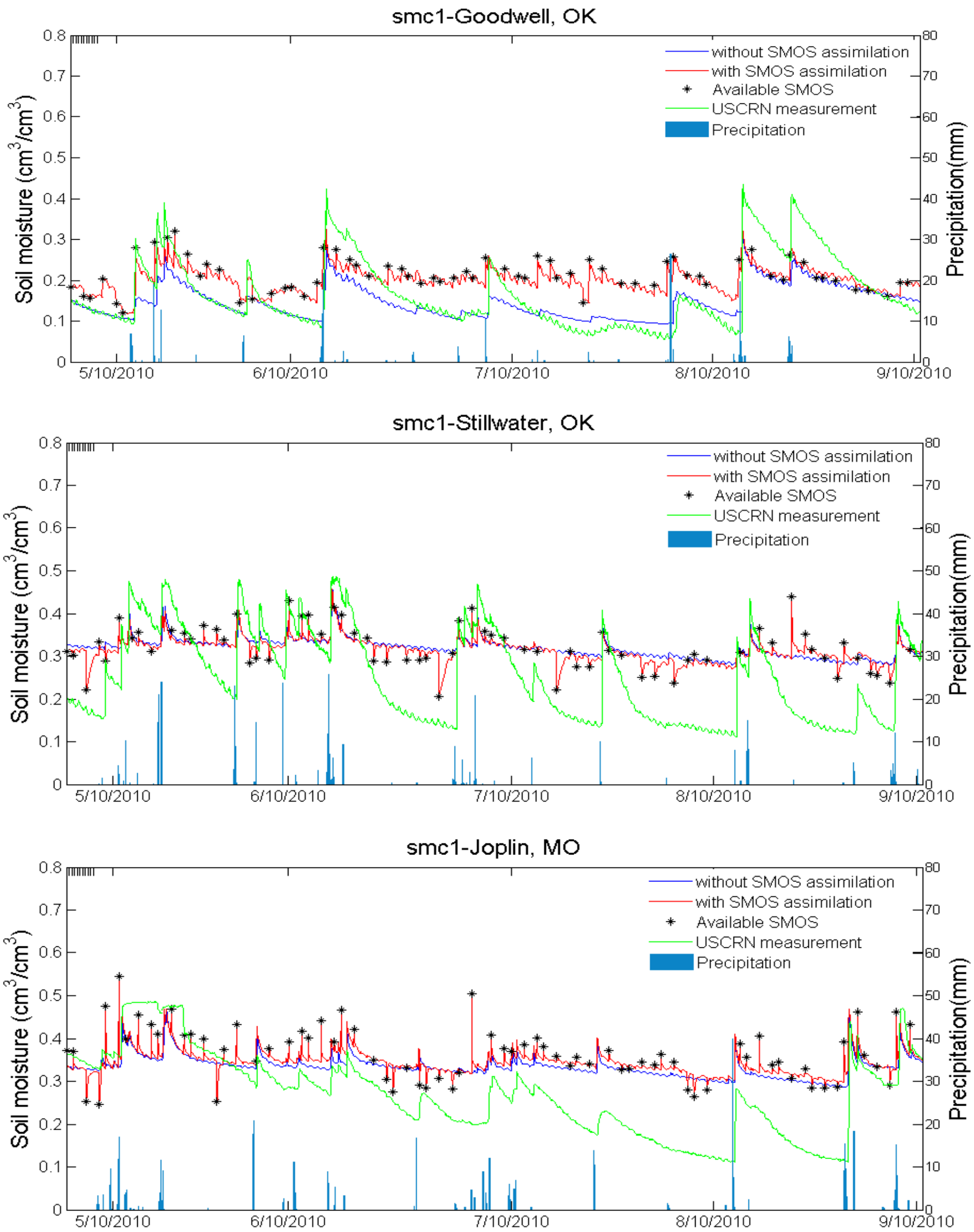

Figure 9 Hourly soil moisture plots of top layer soil moisture from USCRN measurements, HL-RDHM *smc1* output with SMOS assimilation, and without SMOS assimilation from May 2010 to September 2010.

4.2 Performance Statistics

Two analyses are carried out in this section to evaluate the accuracy of SMOS soil moisture and the impact of SMOS assimilation on HL-RDHM soil moisture fields. First, statistical evaluation of SMOS soil moisture data was performed to check the reliability of the data. Root mean square errors (RMSE) were computed for standard and bias-corrected SMOS retrievals using USCRN measurements as a baseline. This analysis revealed that the level of agreement between SMOS retrievals and USCRN measurements differs when the soil is wet versus dry. Accordingly RMSEs were recomputed for two data groups partitioned with a dividing line of 0.3 (Table 2). The RMSEs of the SMOS retrievals (before bias correction) were calculated as 0.07, 0.11, and 0.12 for the Goodwell, Stillwater and Joplin sites respectively. Goodwell, which features -the lowest annual average precipitation (429 mm) and average soil moisture (0.13 cm^3/cm^3) of the three sites, low vegetation cover, sandy -soil texture, and low soil bulk density (1.026 g/cm^3) also has a relatively low RMSE value. This result echoes the findings of other studies (Al Bitar et al., 2012; Jackson et al., 2012; Albergel et al., 2012) which showed that the performance of SMOS depends on soil wetness and vegetation optical depth. The results also indicate that SMOS retrievals perform better when the soil is dry, given the increase in RMSE at all three sites when higher soil moisture cases are examined. Conversely, the bias correction appears to function more effectively for wet cases. Given the soil-moisture dependent performance of the bias correction scheme, future correction methods should be varied based on the level of soil wetness.

Table 2 RMSE of SMOS soil moisture retrievals with and without bias correction for all data and for cases where soil moisture values are greater than 0.3 volumetric.

Sites	Bias of SMOS retrievals	RMSE of SMOS retrievals		RMSE of bias corrected SMOS retrievals	
		All data	Soil moisture > 0.3 (cm^3/cm^3)	All data	Soil moisture > 0.3 (cm^3/cm^3)
Goodwell	- 0.065	0.076	0.155	0.083	0.071
Stillwater	- 0.100	0.111	0.139	0.077	0.034
Joplin	- 0.112	0.120	0.151	0.078	0.049

Using USCRN measurements as a reference, three statistical criteria (RMSE, variance and standard deviation) were next computed to assess the accuracy of HL-RDHM *smc1* soil moisture with and without SMOS assimilation (Figure 9 and Table 3). The results are mixed, with SMOS assimilation leading to slightly increased RMSE at Goodwell and Joplin, and decreased RMSE at the Stillwater site. The standard deviation of the simulated soil moisture increases with SMOS assimilation at the Stillwater and Joplin sites (0.005 and 0.003 respectively) but decreases at Goodwell.

Several explanations can be made for these results. The underlying assumption of the preceding analyses is that the representative measurement depth is similar regardless of the source of the data. However, variations in these depths may have negatively impacted the results. Soil moisture measurements from the USCRN network represent the average value over a depth of 5 to 10 cm, while the effective depth of the HL-RDHM *smc1* soil moisture variable varies pixel to pixel from 5 to 16 cm. The SMOS soil moisture observation depth is assumed to be up to 5 cm, but is relatively uncertain and varies depending on vegetation thickness and soil wetness (Bircher et al., 2012; Dente et al., 2012). Further complicating comparisons, USCRN soil moisture is measured at point while HL-RDHM provides areal-type soil moisture values on a 4 km by 4 km grid. Large differences have been shown to occur between in situ observations only a few meters apart (Collow et al., 2012), making comparisons between point-type and areal-type soil moisture values even more challenging (Jackson et al., 2006).

Although the soil moisture output by HL-RDHM after SMOS assimilation did not precisely match the USCRN measurements, the assimilation of the remotely sensed data did act to shape the model's soil moisture stores, especially on a daily level. Ultimately, the aforementioned uncertainties notwithstanding, satellite-based soil moisture assimilation into HL-RDHM was successfully demonstrated, with a pathway established for inserting soil moisture observations into the model. In addition, the SMOS-assimilation-based increases in SAC-HTET's upper zone saturation ratio in the test case above hints at a potential SMOS-driven improvement in flash flood forecasts. Further case studies are necessary to confirm this limited finding.

Table 3 Statistics (RMSE, variance and standard deviation) of *smc1* comparison between without SMOS assimilation and with SMOS assimilation

Sites	*smc1*-Without SMOS assimilation		*smc1*-With SMOS assimilation	
	RMSE	Standard Deviation	RMSE	Standard Deviation
Goodwell	0.038	0.040	0.069	0.030
Stillwater	0.098	0.023	0.094	0.028
Joplin	0.108	0.025	0.114	0.028

4.3 Comparison of upper zone saturation ratio-GFFG input

The GFFG system uses upper zone saturation ratio (Equation 4) to obtain an adjusted CN value and calculate the available initial abstraction. Differences between the upper zone saturation ratio with and without SMOS assimilation would thus affect the estimation of rainfall depth and runoff needed to cause flash flooding in given unit of time. Therefore, an analysis of *uzsat (upper zone saturation)* speaks directly to the impact of SMOS assimilation on the GFFG system. Toward this end, the upper zone saturation ratio (*uzsat*) was computed using the study data as shown in Equation 4, where *uztwm* is upper zone tension water storage (maximum capacity) and *uzfwm* is upper zone free water storage of HL-RDHM:

$$\boldsymbol{uzsat = \frac{(uztwc \times uztwm)+(uzfwc \times uzfwm)}{uztwm+uzfwm}} \qquad \text{Equation 4}$$

The higher *uzsat* values resulting from SMOS assimilation in this study case, and illustrated in Figure 10, highlight the potential for improving flash flood detection via improved GFFG values. For example, through an investigation of the NWS flash flood event database (Seo et al., 2013), it was found that flash flooding occurred in Newton and McDonald Counties of Missouri (latitude 36.93°, longitude -94.44°), an area near to the Joplin study site (latitude 37.43°, longitude -94.58°), on May 16th, 2010. This flood date coincides with the first *uzsat* peak on the Joplin plot, circled in purple in Figure 10. In this graph, the red line (with SMOS assimilation) reaches a value of 1, while the blue line (without SMOS assimilation) tops out at about 0.85. According to archived GFFG data on that day, the pixel values of GFFG corresponding to Newton and McDonald County were 2.59 inches for 6 hours, meaning that flash flooding could be expected if 2.59 inches of rain fell in 6 hours or less. However, flash flooding occurred when the 6-hour rainfall reached only

0.29 inches after the GFFG was issued. The higher value of *uzsat* in the with-SMOS HL-RDHM simulation would have led to lower computed GFFG values and thus an indication of the increased potential for flash flooding.

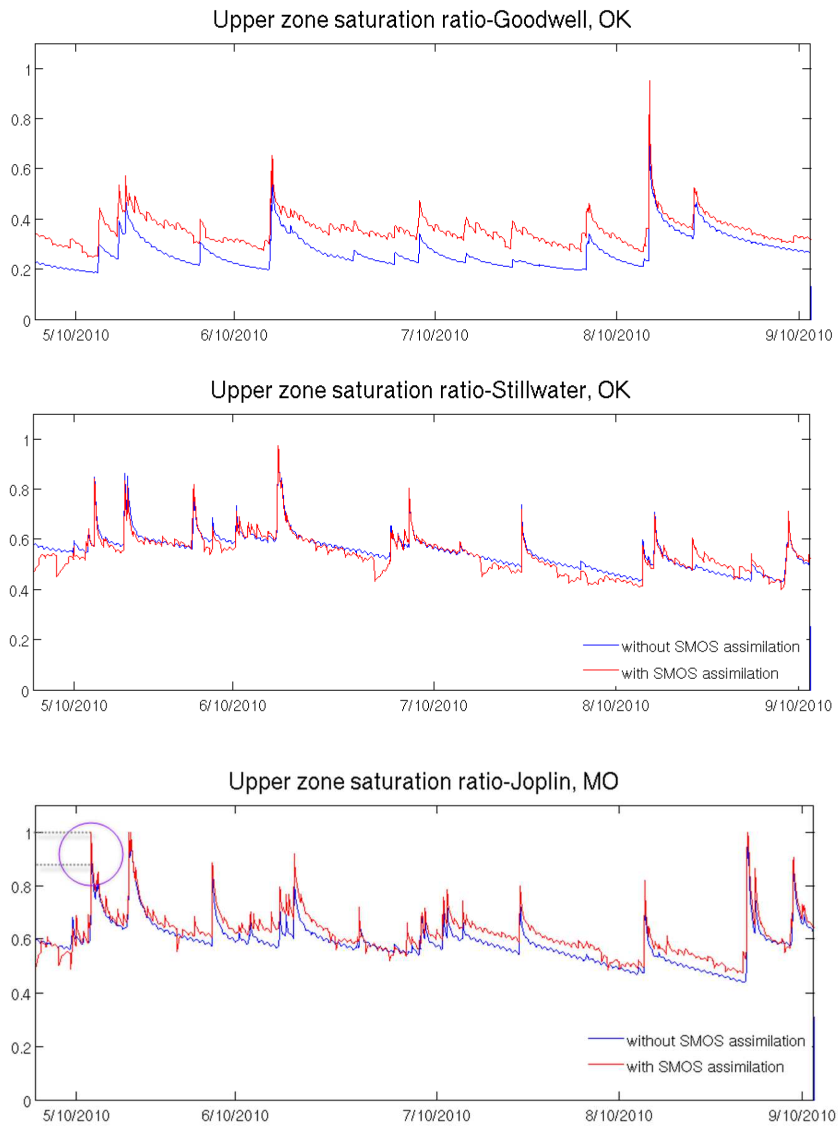

Figure 10 Hourly upper zone saturation ratio calculated from HL-RDHM's *uztwc, uztwm, uzfwc*, and *uzfwm* with SMOS assimilation (red line) and without SMOS assimilation (blue line)

5 Summary and Conclusion

The goal of this study was to develop an approach to assimilate satellite-based soil moisture data into the NWS's HL-RDHM hydrologic modeling system, thus supporting a downstream improvement in the GFFG product. The impact of soil moisture information on flash flood forecasts was discussed and the detailed technique of SMOS soil moisture data assimilation, including spatial scaling and bias adjustment, was described. SMOS soil moisture data was assimilated into the *smc1* layer of the SAC-HTET model using the direct insertion technique, a SAC-HTET function was utilized to translate soil moisture content in the model's top physical layer to the model's upper and lower zone conceptual storage reservoirs. Missing SMOS pixels were replaced with HL-RDHM *smc1* model-based values valid at the same time.

An investigation into the impact of SMOS assimilation on HL-RDHM soil moisture states *smc1, uztwc, uzfwc*, and the upper zone saturation ratio was carried out. Soil wetness variations in the SMOS data were reasonably translated to HL-RDHM, although a short persistence time was noted. Given the direct link between *uzsat* and GFFG values, it was also noted that the higher HL-RDHM *uzsat* values caused by SMOS assimilation would have improved the potential for a correct flash flood forecast in the case study. Additional case studies need to be conducted to further define the extent of this GFFG benefit.

The accuracy of SMOS observed soil moisture varies with the characteristics of the underlying soil, vegetation and geography. At the three study sites (Goodwell, Stillwater, and Joplin), it was found that the magnitude of the bias in SMOS measurements depends on the soil dryness and vegetation cover, with better performance found for relatively dry and bare soil. As such, a refinement of both the soil moisture retrieval algorithm and the bias correction method applied in this study may contribute to more accurate soil moisture estimations from SMOS. Overall, a simple technique for assimilating satellite based soil moisture into the HL-RDHM hydrologic modeling system was successfully developed. In addition, a potential improvement of GFFG, and thus flash flood forecasts, was seen to result from the assimilation of SMOS data, paving the way for further studies in this area. The assimilation technique developed in this study is expected to benefit a wide range of hydrologic modeling applications, and should prove useful for assimilating forthcoming SMAP data as well.

ACKNOWLEDGEMENT

This study was supported and monitored by National Oceanic and Atmospheric Administration (NOAA) under Grant NA06OAR4810162 and NA11SEC4810004. The views, opinions, and findings contained in this report are those of the authors and should not be construed as an official National Oceanic and Atmospheric Administration or U.S. Government position, policy, or decision. The authors thank to Zhengtao Cui and Mike Smith from NOAA-National Weather Service, Office of Hydrologic Development for useful comments and suggestions in preparation of this manuscript. Comments and suggestions from two anonymous reviewers and member of the Editorial Board were extremely valuable in creating the final version of this manuscript.

REFERENCES

Al Bitar, A., Leroux, D., Kerr, Y. H., Merlin, O., Richaume, P., Sahoo, A., & Wood, E. F. (2012). Evaluation of SMOS Soil Moisture Products Over Continental U.S. Using the SCAN/SNOTEL Network. *IEEE Transactions on Geoscience and Remote Sensing*. http://doi.org/10.1109/TGRS.2012.2186581

Albergel, C., de Rosnay, P., Gruhier, C., Muñoz-Sabater, J., Hasenauer, S., Isaksen, L., … Wagner, W. (2012). Evaluation of remotely sensed and modelled soil moisture products using global ground-based in situ observations. *Remote Sensing of Environment*. http://doi.org/10.1016/j.rse.2011.11.017

Bell, J. E., M. A. Palecki, C. B. Baker, W. G. Collins, J. H. Lawrimore, R. D. Leeper, M. E. Hall, J. Kochendorfer, T. P. Meyers, T. Wilson, and H. J. D. (2013). U.S. Climate Reference Network soil moisture and temperature observations. *J. Hydrometeorol*, *14*, 977–988. Retrieved from doi: 10.1175/JHM-D-12-0146.1

Bircher, S., Skou, N., Jensen, K. H., Walker, J. P., & Rasmussen, L. (2012). A soil moisture and temperature network for SMOS validation in Western Denmark. *Hydrology and Earth System Sciences*, *16*(5), 1445–1463. http://doi.org/10.5194/hess-16-1445-2012

Bruckler, L. and Witono, H. (1989). Use of remotely sensed soil moisture content as boundary conditions in soil-atmosphere water transport modeling 2: Estimating soil water balance. *Water Resource Research*, *25*, 2437–2447.

Burnash, R. J. C. (1995). *The NWS river forecast system-catchment modeling. Computer Models of Watershed Hydrology*. (V. P. Singh, Ed.). Littleton, CO: Water Resources Publications.

Choi, M., & Jacobs, J. M. (2008). Temporal Variability Corrections for Advanced Microwave Scanning Radiometer E (AMSR-E) Surface Soil Moisture: Case Study in Little River Region, Georgia, U.S. *Sensors*, *8*(4), 2617–2627. http://doi.org/10.3390/s8042617

CROW, W., KUSTAS, W., & PRUEGER, J. (2008). Monitoring root-zone soil moisture through the assimilation of a thermal remote sensing-based soil moisture proxy into a water balance model. *Remote Sensing of Environment*. http://doi.org/10.1016/j.rse.2006.11.033

Das N.N., Mohanty B.P., Efendiev Y., S. D. (2014). Data-driven downscaling of satellite-based surface soil moisture data using high resolution physical controls information. *Water Resources Research*, *In Review*.

Dente, L., Su, Z., & Wen, J. (2012). Validation of SMOS soil moisture products over the Maqu and Twente regions. *Sensors (Basel, Switzerland)*, *12*(8), 9965–86. http://doi.org/10.3390/s120809965

Diamond, H. J., Karl, T. R., Palecki, M. a., Baker, C. B., Bell, J. E., Leeper, R. D., … Thorne, P. W. (2013). U.S. Climate Reference Network after One Decade of Operations: Status and Assessment. *Bulletin of the American Meteorological Society*, *94*(4), 485–498. http://doi.org/10.1175/BAMS-D-12-00170.1

Entekhabi, D., Nakamura, H., & Njoku, E. G. (1994). Solving the inverse problem for soil moisture and temperatureprofiles by sequential assimilation of multifrequency remotely sensedobservations. *IEEE Transactions on Geoscience and Remote Sensing*, *32*(2).

http://doi.org/10.1109/36.295058

Entekhabi, D., Njoku, E. G., O'Neill, P. E., Kellogg, K. H., Crow, W. T., Edelstein, W. N., … Zyl, J. Van. (2010). The Soil Moisture Active Passive (SMAP) Mission. *Proceedings of the IEEE*, *98*(5).

Escorihuela, M. J., Chanzy, A., Wigneron, J. P., & Kerr, Y. H. (2010). Effective soil moisture sampling depth of L-band radiometry: A case study. *Remote Sensing of Environment*. http://doi.org/10.1016/j.rse.2009.12.011

Gruntfest, E. (2009). Editorial. *Journal of Flood Risk Management*, *2*(2), 83–84. http://doi.org/10.1111/j.1753-318X.2008.00019.x

Henninger, D. L., Petersen, G. W., & Engman, E. T. (1976). Surface Soil Moisture within a Watershed—Variations, Factors Influencing, and Relationship to Surface Runoff1. Retrieved from https://www.agronomy.org/publications/sssaj/abstracts/40/5/773

Houser, P. R., Shuttleworth, W. J., Famiglietti, J. S., Gupta, H. V, Syed, K. H., & Goodrich, D. C. (1998). Integration of soil moisture remote sensing and hydrologic modeling using data assimilation. *Water Resources Research*, *34*(12), 3405–3420. http://doi.org/10.1029/1998WR900001

Jackson, T. J., Bindlish, R., Cosh, M. H., Zhao, T., Starks, P. J., Bosch, D. D., … Leroux, D. (2012). Validation of Soil Moisture and Ocean Salinity (SMOS) Soil Moisture Over Watershed Networks in the U.S. *IEEE Transactions on Geoscience and Remote Sensing*. http://doi.org/10.1109/TGRS.2011.2168533

Jackson, T. J., Cosh, M. H., Zhan, X., Bosch, D. D., Seyfried, M. S., Starks, P. J., … Lakshmi, V. (2006). Validation of AMSR-E Soil Moisture Products Using Watershed Networks. *Geoscience and Remote Sensing Symposium, 2006. IGARSS 2006. IEEE International Conference on*. http://doi.org/10.1109/IGARSS.2006.115

Jackson, T. J., Vine, D. M. Le, Hsu, A. Y., Oldak, A., Starks, P. J., Swift, C. T., … Haken, M. (1999). Soil moisture mapping at regional scales using microwaveradiometry: the Southern Great Plains Hydrology Experiment. *IEEE Transactions on Geoscience and Remote Sensing*, *37*(5). http://doi.org/10.1109/36.789610

Jackson, T. J., Vine, D. M. Le, Swifi, C. T., Schmugge, T. J., & Schiebe, F. R. (1995). Large Area Mapping of Soil Moisture Using the ESTAR Passive Microwave Radiometer in Washita â€™ 92. *Remote Sensing of Environment*, *54*(1), 27–37. http://doi.org/10.1016/0034-4257(95)00084-E

Kaheil, Y. H., Gill, M. K., McKee, M., Bastidas, L. A., & Rosero, E. (2008). Downscaling and Assimilation of Surface Soil Moisture Using Ground Truth Measurements. *IEEE Transactions on Geoscience and Remote Sensing*. http://doi.org/10.1109/TGRS.2008.916086

Kerr, Y. H., Waldteufel, P., Richaume, P., Wigneron, J. P., Ferrazzoli, P., Mahmoodi, A., … Delwart, S. (2012). The SMOS Soil Moisture Retrieval Algorithm. *IEEE Transactions on Geoscience and Remote Sensing*. http://doi.org/10.1109/TGRS.2012.2184548

Kerr, Y. H., Waldteufel, P., Wigneron, J.-P., Martinuzzi, J., Font, J., & Berger, M. (2001). Soil moisture retrieval from space: the Soil Moisture and Ocean Salinity (SMOS) mission.

Geoscience and Remote Sensing, IEEE Transactions on. http://doi.org/10.1109/36.942551

KERR Y., WALDTEUFEL P., WIGNERON J.-P., DELWART S., CABOT F., BOUTIN J., … S. (2010). The SMOS mission: new tool for monitoring key elements of the global water cycle. *Proceedings of the IEEE*, *98*, *Specia*(5), 666–687. Retrieved from http://dx.doi.org/10.1109/JPROC.2010.2043032

Ko, A., Mascaro, G., & Vivoni, E. R. (2016). Irrigation Impacts on Scaling Properties of Soil Moisture and the Calibration of a Multifractal Downscaling Model. *IEEE Transactions on Geoscience and Remote Sensing*. http://doi.org/10.1109/TGRS.2015.2511628

Koren, V., Smith, M., Cui, Z., Cosgrove, B. (2010). *Modification of Sacramento Soil Moisture Accounting Heat Transfer Component (SAC-HT) for Enhanced Evapotranspiration*.

Koren, V., Reed, S., Smith, M., Zhang, Z., & Seo, D. J. (2004). Hydrology Laboratory Research Modeling System (HL-RMS) of the US National Weather Service. *Journal of Hydrology*, *291*(3–4), 297–318.

Koren, V., Smith, M., Cui, Z., Cosgrove, B., Werner, K., & Zamora, R. (2010). *Modification of Sacramento Soil Moisture Accounting Heat Transfer Component (SAC-HT) for Enhanced Evapotranspiration*.

Lee, K., Burke, E. J., Shuttleworth, W., & Harlow, R. (2002). Influence of vegetation on SMOS mission retrievals. *Hydrology and Earth System Sciences*. http://doi.org/10.5194/hess-6-153-2002

Lievens, H., De Lannoy, G. J. M., Al Bitar, A., Drusch, M., Dumedah, G., Hendricks Franssen, H.-J., … Pauwels, V. R. N. (2016). Assimilation of SMOS soil moisture and brightness temperature products into a land surface model. *Remote Sensing of Environment*, *180*, 292–304. http://doi.org/https://doi.org/10.1016/j.rse.2015.10.033

Lievens, H., Tomer, S. K., Al Bitar, A., De Lannoy, G. J. M., Drusch, M., Dumedah, G., … Pauwels, V. R. N. (2015). SMOS soil moisture assimilation for improved hydrologic simulation in the Murray Darling Basin, Australia. *Remote Sensing of Environment*, *168*, 146–162. http://doi.org/https://doi.org/10.1016/j.rse.2015.06.025

Mascaro, G., & Vivoni, E. R. (2012). Utility of coarse and downscaled soil moisture products at L-band for hydrologic modeling at the catchment scale. *Geophysical Research Letters*, *39*(10), n/a-n/a. http://doi.org/10.1029/2012GL051809

Mascaro, G., Vivoni, E. R., & Deidda, R. (2010). Downscaling soil moisture in the southern Great Plains through a calibrated multifractal model for land surface modeling applications. *Water Resources Research*, *46*(8), 1–18. http://doi.org/10.1029/2009WR008855

Merlin, O., Chehbouni, A., Kerr, Y. H., & Goodrich, D. C. (2006). A downscaling method for distributing surface soil moisture within a microwave pixel: Application to the Monsoon '90 data. *Remote Sensing of Environment*, *101*(3), 379–389. http://doi.org/10.1016/j.rse.2006.01.004

Pan, M., Sahoo, A. K., Wood, E. F., Al Bitar, A., Leroux, D., & Kerr, Y. H. (2012). An Initial Assessment of SMOS Derived Soil Moisture over the Continental United States. *IEEE Journal of Selected Topics in Applied Earth Observations and Remote Sensing*. http://doi.org/10.1109/JSTARS.2012.2194477

Pellenq, J., Kalma, J., Boulet, G., Saulnier, G.-M., Wooldridge, S., Kerr, Y., & Chehbouni, A. (2003). A disaggregation scheme for soil moisture based on topography and soil depth. *Journal of Hydrology*, *276*(1–4), 112–127. http://doi.org/10.1016/S0022-1694(03)00066-0

Piles, M. X. E. A., Camps, A., Vall-llossera, M. X. E., Corbella, I., Panciera, R., Rudiger, C., … Walker, J. (2011). Downscaling SMOS-Derived Soil Moisture Using MODIS Visible/Infrared Data. *IEEE Transactions on Geoscience and Remote Sensing*. IEEE. Retrieved from http://ieeexplore.ieee.org/lpdocs/epic03/wrapper.htm?arnumber=5756664

Seo, D., Tarendra, L., Cosgrove, B., & Khabilvardi, R. (2013). Evaluation of Operational National Weather Service Gridded Flash Flood Guidance over the Arkansas Red River Basin. *JAWRA Journal of the American Water Resources Association*, *49*(6), 1296–1307.

Shin, Y., & Mohanty, B. P. (2013). Development of a deterministic downscaling algorithm for remote sensing soil moisture footprint using soil and vegetation classifications. *Water Resources Research*, *49*(10), 6208–6228. http://doi.org/10.1002/wrcr.20495

Thomas W. Collow, Alan Robock, Jeffrey B. Basara, B. G. I. (2012). Evaluation of SMOS retrievals of soil moisture over the central United States with currently available in situ observations. *Journal of Geophysical Research*, *117*(D09113).

Ulaby, F. T., Moore, R. K., & Fung, A. K. (1981). Microwave remote sensing: Active and passive. Volume 1 - Microwave remote sensing fundamentals and radiometry. *Microwave Remote Sensing Active and Passive*, *1*(1), 456.